Electronic Supplementary Information (ESI)

Polymer-Assisted Synthesis of Mixed-Halide Quasi-2D Perovskites for Tunable Blue-Green Lasers

Yuanyi Li,[a] *Haihua Zhang,**[a] *Hongbing Fu**[ab]

[a] Institute of Molecular Plus (IMP), Collaborative Innovation Center of Chemical Science and Engineering (Tianjin), National Industry-Education Platform for Energy Storage (Tianjin), Tianjin University, Tianjin 300072, P. R. China.

[b] Beijing Key Laboratory for Optical Materials and Photonic Devices, Department of Chemistry, Capital Normal University, Beijing 100048, P. R. China

* Email: zhanghaihua@tju.edu.cn; hbfu@cnu.edu.cn

KEYWORDS: Quasi-2D perovskite, Quantum well, Optical gain, Blue-green Laser

Experimental Section

1. **Materials:** Lead bromide ($PbBr_2$, 99.99%), cesium bromide (CsBr, 99.99%), butylammonium bromide (BABr, 99.5%), cesium chloride (CsCl, 99.5%), and lead chloride ($PbCl_2$, 99.999%) were purchased from Xi'an Polymer Light Technology Corp and used as received without further purification. Dimethyl sulfoxide (DMSO), and Polyvinyl pyrrolidone (PVP) were purchased from Beijing InnoChem Science & Technology Co., Ltd.

2. **PVP-modified Quasi-2D Perovskite thin films preparation:** The PVP-modified quasi-2D perovskite $BA_2Cs_{n-1}Pb_nX_{3n+1}$ (n = 5) films were synthesized using a one-step spin-coating method in a nitrogen-filled glovebox. The BABr, CsBr, $PbBr_2$, CsCl and $PbCl_2$ was dissolved in DMSO solvent to prepare starting solution (maintain Pb^{2+} concentration of 0.15 mol/L). 10 mg/mL PVP was added to the precursor solution. The obtained perovskite precursor solution was spin-coated onto the substrates via spin coating process at 3000 rpm for 60 s. Then the perovskite films were annealed at 60 °C for 5 min. Mixed-halide perovskite films were obtained by varying the precursor solution constitution following a similar strategy.

3. **Morphology and spectra measurements:** The morphologies using field emission scanning electron microscopy (FESEM, Thermo Fisher Scientific) at acceleration voltages of 10 kV. UV-vis absorption spectra were obtained from a Thermo Fisher Scientific Evolution 201. PL spectra were measured on an Edinburgh FLS1000 spectrometer. The bonding energy of Pb, Br and Cl was tested by an X-ray photoelectron spectrometer (XPS, K-Alpha+). X-ray diffraction patterns were measured by a D/max 2500 X-ray diffractometer with Cu Kα radiation (λ = 1.54050 Å) operated in the 2θ range from 5 to 40.

4. **TA Measurements:** A femtosecond laser system·(Pharos, Light·Conversion)delivered laser pulses at-1030 nm·(180 fs, 6 kHz), which were then divided into two components by using a 9:1 beam splitter. The major component was sent to an optical parametric amplifier. (Orpheus, Light Conversion) to generate the pump pulses·(370 nm, 6 kHz). The minor component was further attenuated and focused into a·3-mm·sapphire plate to generate the probe pulses. Both the pump and probe pulses were guided into a Harppa spectrometer and time resolved spectral data were recorded. A·short-pass filter was inserted into the probe beam to·cut off the fundamental light of 1030 nm. The time delay between the pump and probe beams were regulated through·a computer-controlled motorized translation stage in the probe beam. The temporal resolution between the pump and the probe pulses was·determined to be ~200 fs (FWHM). The transmitted light was detected by a CMOS linear image sensor. Analysis of the kinetic traces derived from time-resolved spectra was performed using nonlinear least-square fitting to a general sum-of-exponentials function after deconvolution of instrument response funciton (IRF). All the spectroscopic measurements were carried out at room temperature.

5. **ASE Measurements:** For the ASE measurements, the laser pulses from the femtosecond laser system (Pharos, Light Conversion) delivered at 1030 nm(180 fs, 6 kHz), which were then divided into two components using a 9:1 beam splitter. The major component was sent to an optical parametric amplifier (Orpheus, Light Conversion) to generate the pump pulses (400 nm, 6 kHz). These pump pulses were then focused vertically onto the PVP-modified $BA_2Cs_{n-1}Pb_nX_{3n+1}$ film with dimension of ~0.1×1.5 mm^2 via a cylindrical lens, and the emission from the edge of the film serving as the optical waveguide was vertically collected and detected with a liquid-nitrogen-cooled CCD (Isoplane320, Rrineenton Instuments) attached to a polychromator (Spectropro-550i, Acton).

6. **Laser Measurements:** The PVP-modified $BA_2Cs_{n-1}Pb_nX_{3n+1}$ micro-ring arrays were performed on a home-made inverted fluorescence microscopy equipped with a 40× objective. The optical. parametric amplifier (Orpheus, Light Conversion, 400 nm,6 kHz) was focused to a 200-μm-diameter spot. The PL spectra were collected in a reflection mode with a movable aperture on the optical path at the front focal plane, collected and detected with a liquid-nitrogen-cooled CCD (nanosecond-pulsed laser system, excitation wavelength: 355 nm, pulse width: 7 ns, repetition rate: 20 Hz).

7. Addition sections

Fig. S1

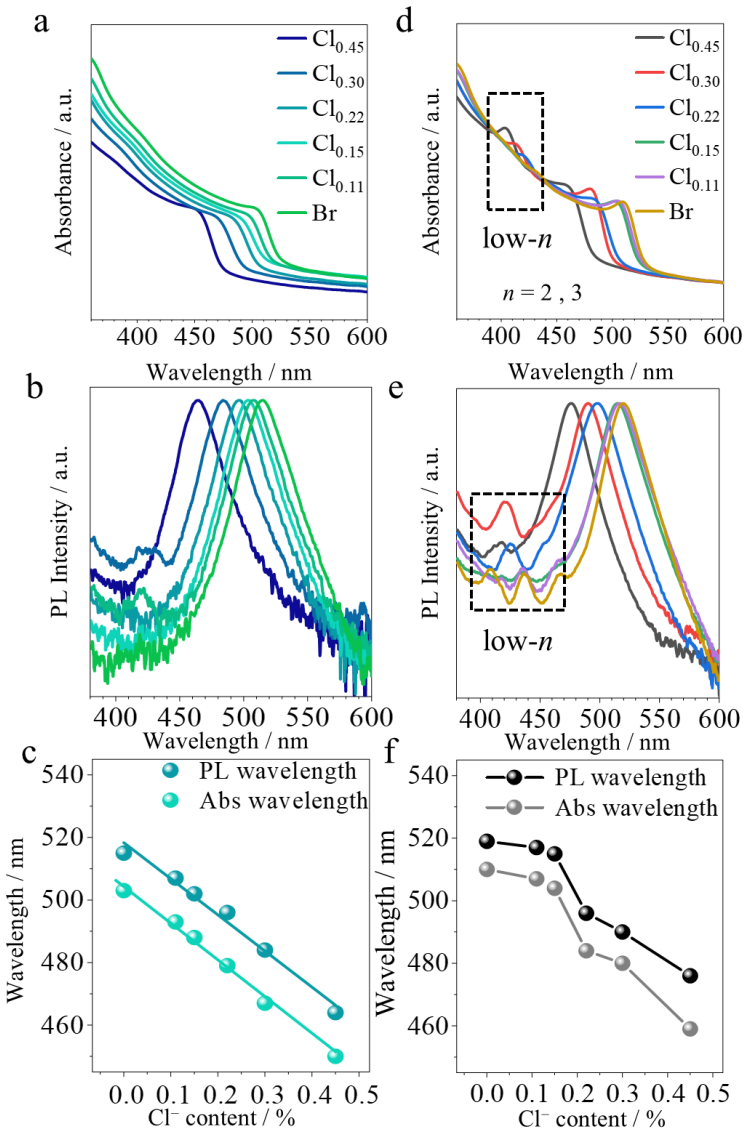

Fig. S1 (a-b) Steady-state absorption and PL spectra of PVP-modified $BA_2Cs_{n-1}Pb_nX_{3n+1}$ (n = 5) films with varying Cl/Br ratio. (d-e) Absorption and PL spectra of pristine $BA_2Cs_{n-1}Pb_nX_{3n+1}$ films. Correlation between wavelength of PL peak, band edge absorption and chlorine content of PVP-modified (c) and pristine (f) $BA_2Cs_{n-1}Pb_nX_{3n+1}$ films, respectively.

Fig. S2

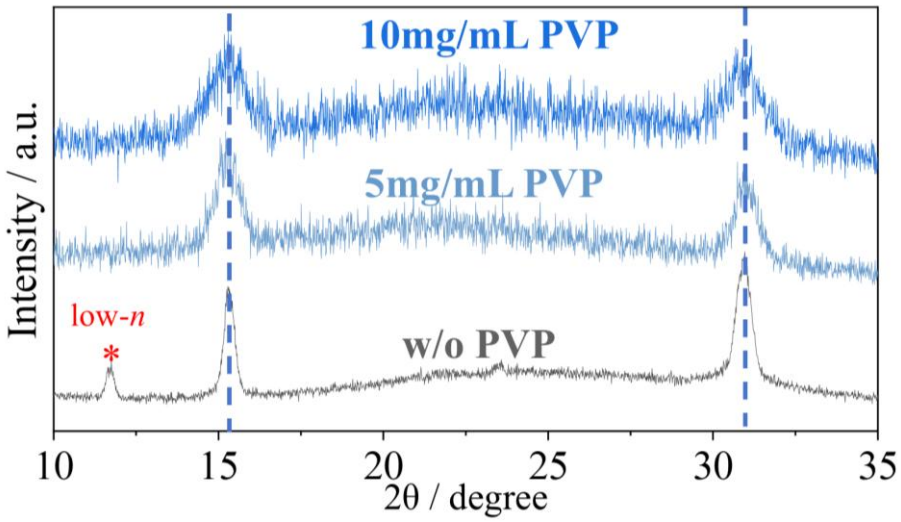

Fig. S2 The XRD patterns of pristine and PVP-modified $BA_2Cs_{n-1}Pb_nX_{3n+1}$ films.

Fig. S3

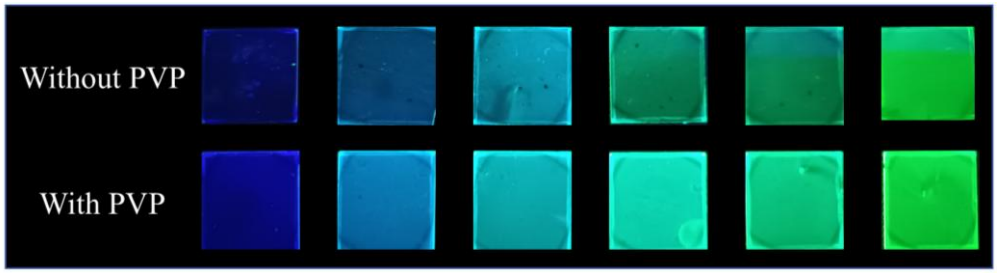

Fig. S3 PL image of pristine and PVP-modified quasi-2D perovskite $BA_2Cs_{n-1}Pb_nX_{3n+1}$ thin films under 365 nm UV excitation.

Fig. S4

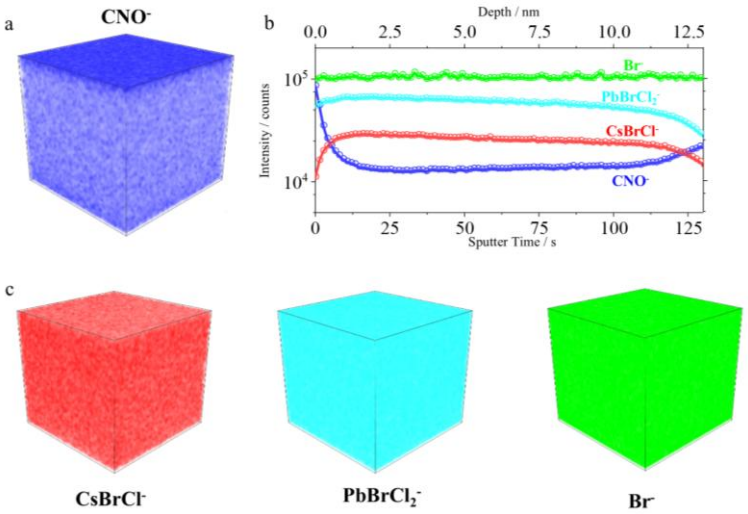

Fig. S4 (a) The 3D TOF-SIMS profile mapping of the CNO^- distribution. (b) TOF-SIMS depth profiles of functional groups in the $Cl_{0.15}Br_{0.85}$ film. (c) The 3D TOF-SIMS profile mapping of the $CsBrCl^-$, $PbBrCl_2^-$ and Br^- distributions.

Fig. S5

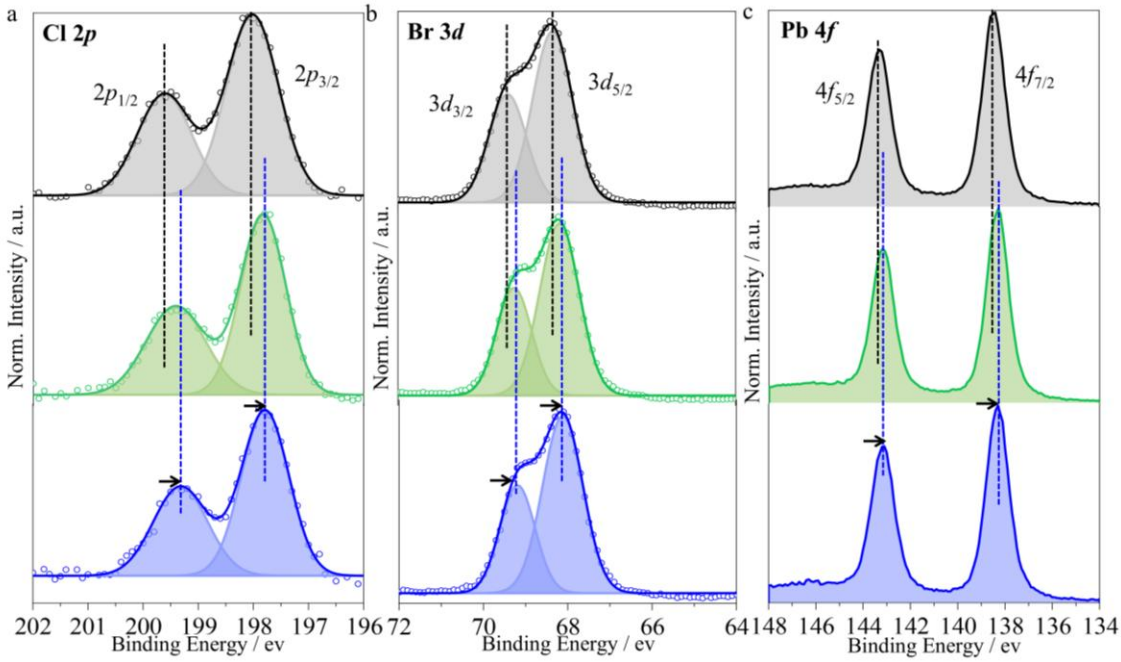

Fig. S5 (a-c) XPS spectra (Cl 2p, Br 3d and Pb 4f) of the pristine sample and PVP-modified films (green: 5 mg/mL PVP, blue: 10 mg/mL PVP).

Fig. S6

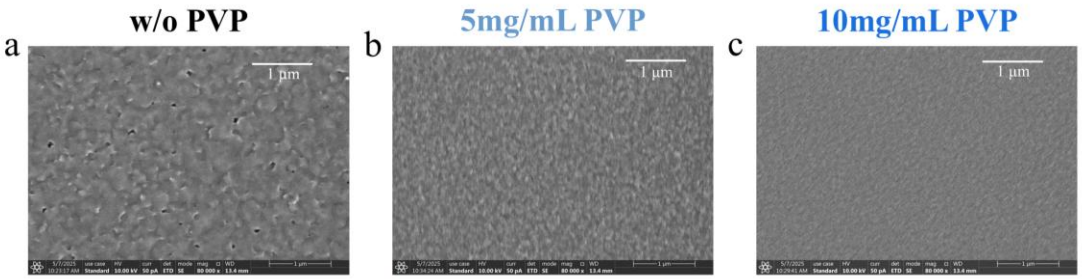

Fig. S6 (a-c) The SEM images of pristine and PVP-modified $BA_2Cs_{n-1}Pb_nX_{3n+1}$ films.

Fig. S7

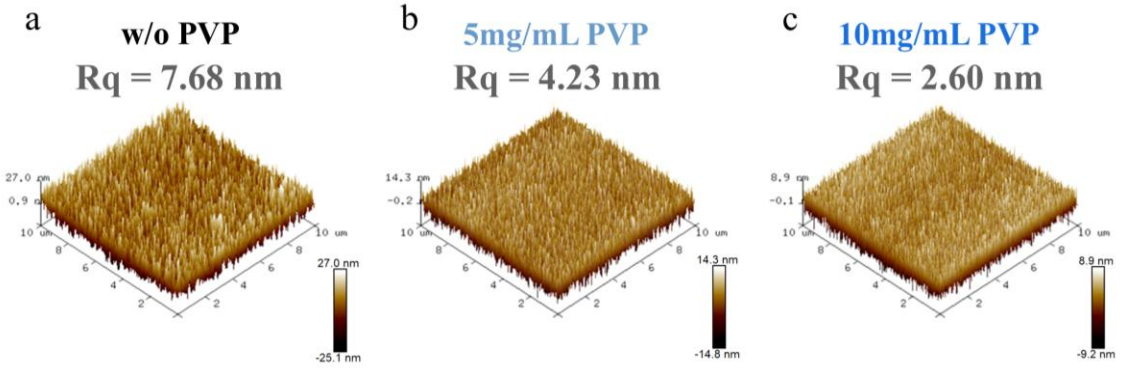

Fig. S7 (a-c) The AFM images of pristine and PVP-modified $BA_2Cs_{n-1}Pb_nX_{3n+1}$ films.

Fig. S8

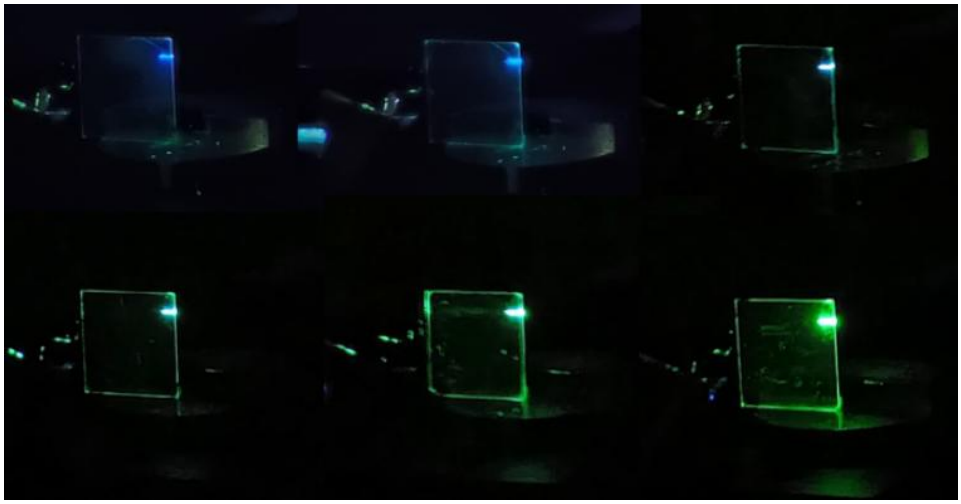

Fig. S8 Optical images of PVP-modified $BA_2Cs_{n-1}Pb_nX_{3n+1}$ films.

Fig. S9

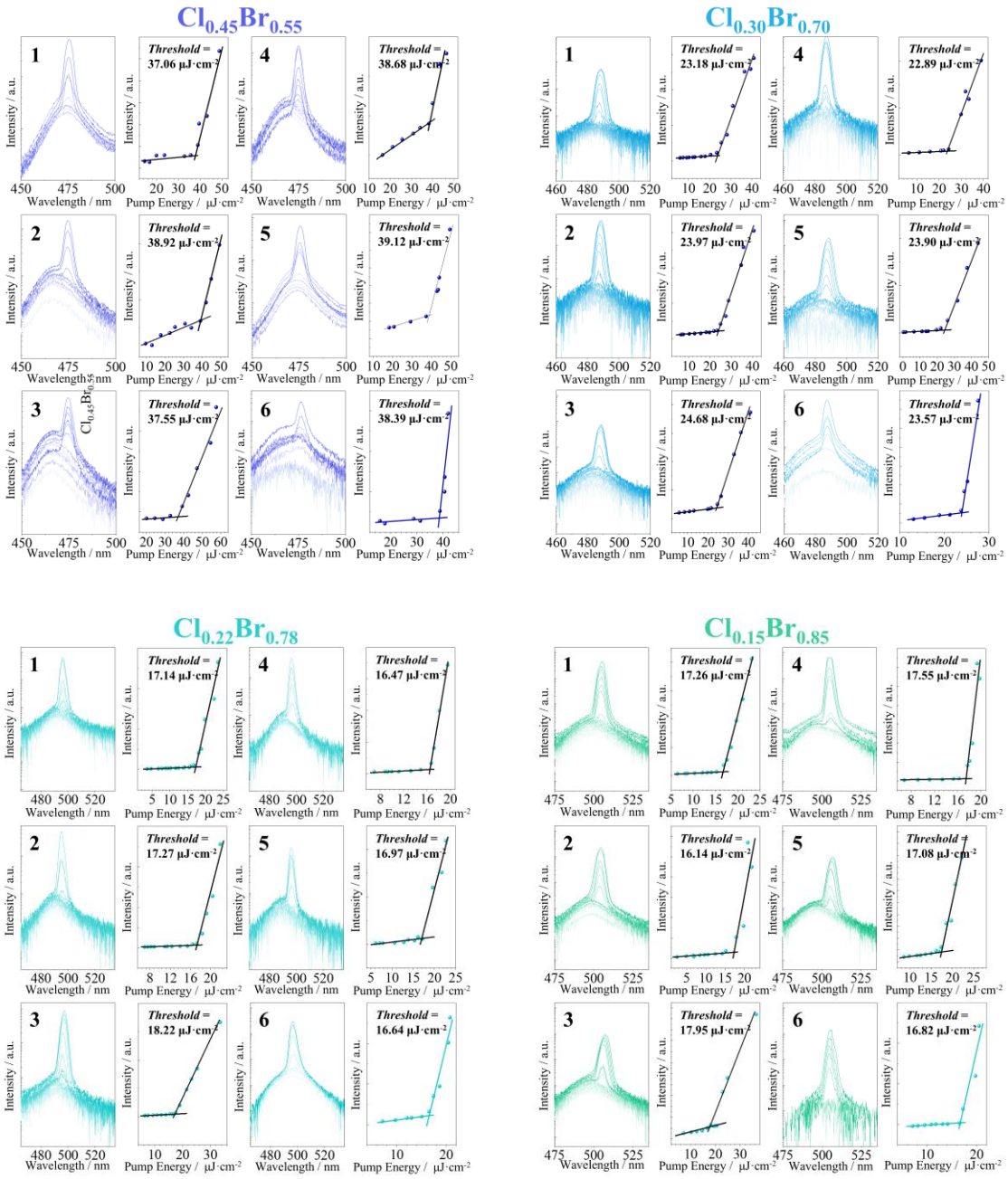
Cl0.45Br0.55
Threshold = 37.06 μJ·cm-2
Threshold = 38.68 μJ·cm-2
Threshold = 38.92 μJ·cm-2
Threshold = 39.12 μJ·cm-2
Threshold = 37.55 μJ·cm-2
Threshold = 38.39 μJ·cm-2
Cl0.30Br0.70
Threshold = 23.18 μJ·cm-2
Threshold = 22.89 μJ·cm-2
Threshold = 23.97 μJ·cm-2
Threshold = 23.90 μJ·cm-2
Threshold = 24.68 μJ·cm-2
Threshold = 23.57 μJ·cm-2
Cl0.22Br0.78
Threshold = 17.14 μJ·cm-2
Threshold = 16.47 μJ·cm-2
Threshold = 17.27 μJ·cm-2
Threshold = 16.97 μJ·cm-2
Threshold = 18.22 μJ·cm-2
Threshold = 16.64 μJ·cm-2
Cl0.15Br0.85
Threshold = 17.26 μJ·cm-2
Threshold = 17.55 μJ·cm-2
Threshold = 16.14 μJ·cm-2
Threshold = 17.08 μJ·cm-2
Threshold = 17.95 μJ·cm-2
Threshold = 16.82 μJ·cm-2
Intensity / a.u.
Wavelength / nm
Pump Energy / μJ·cm-2

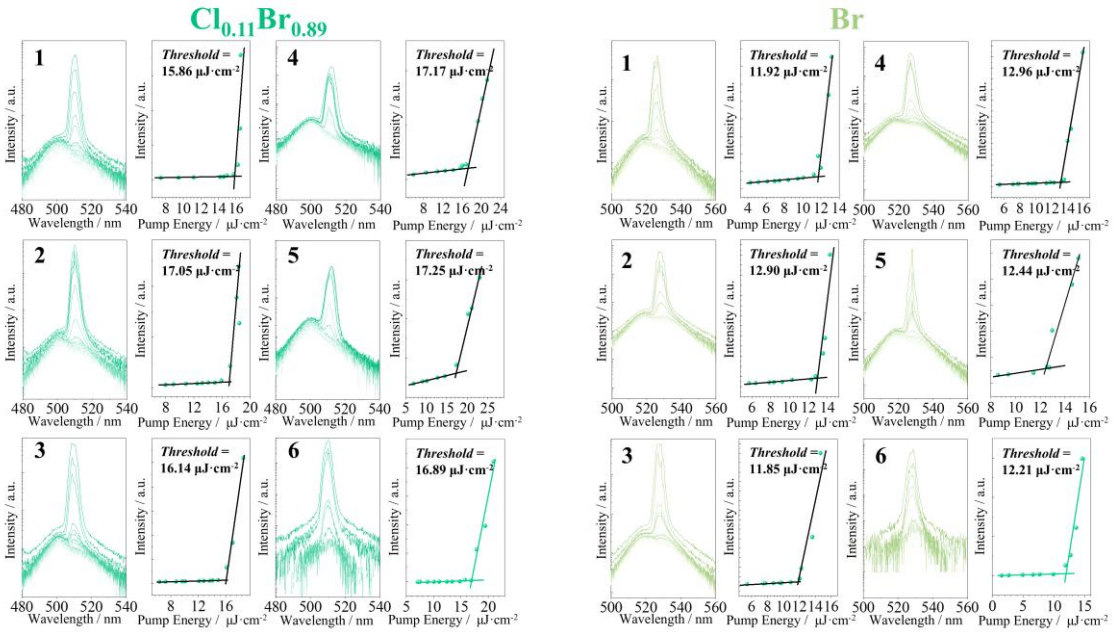

Fig. S9 Pump-fluence dependent PL intensity of different Cl^-/Br^- ratios films at 400 nm excitation and the plot of integrated PL intensities versus pump density of different Cl^-/Br^- ratios films. (there are six groups of $Cl_{0.45}Br_{0.55}$, $Cl_{0.30}Br_{0.70}$, $Cl_{0.22}Br_{0.78}$, $Cl_{0.15}Br_{0.85}$, $Cl_{0.11}Br_{0.89}$ and pure Br).

Fig. S10

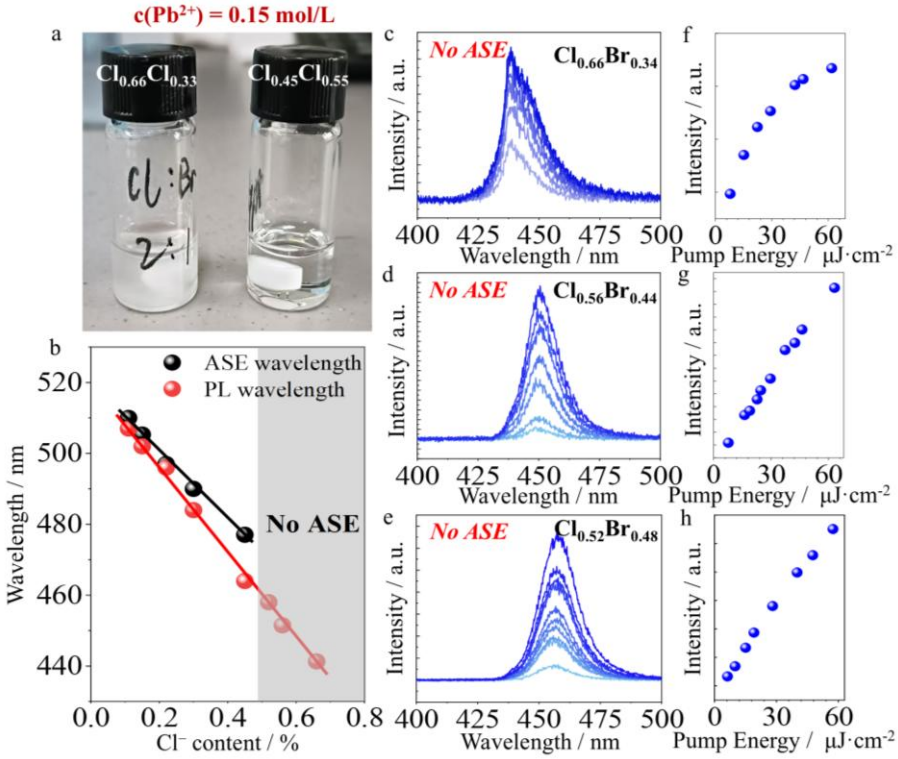

Fig. S10 (a) Optical images of precursor solution of mixed-halide perovskite ($Cl_{0.66}Br_{0.34}$ could not dissolve completely). (b) Correlation between Cl^- content and ASE/PL wavelength of PVP-modified $BA_2Cs_{n-1}Pb_nX_{3n+1}$ films. (c-h) Pump-fluence-dependent PL intensity of X= $Cl_{0.66}Br_{0.34}$, $Cl_{0.56}Br_{0.44}$ and $Cl_{0.52}Br_{0.48}$ films.

Fig. S11

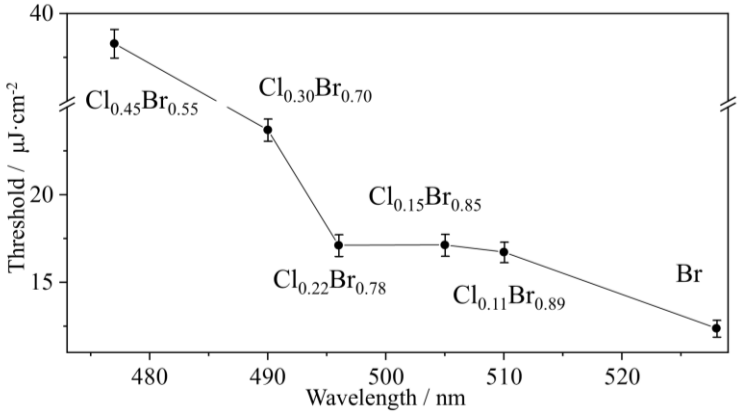

Fig. S11 Summary of the ASE thresholds of the PVP-modified $BA_2Cs_{n-1}Pb_nX_{3n+1}$ films.

Fig. S12

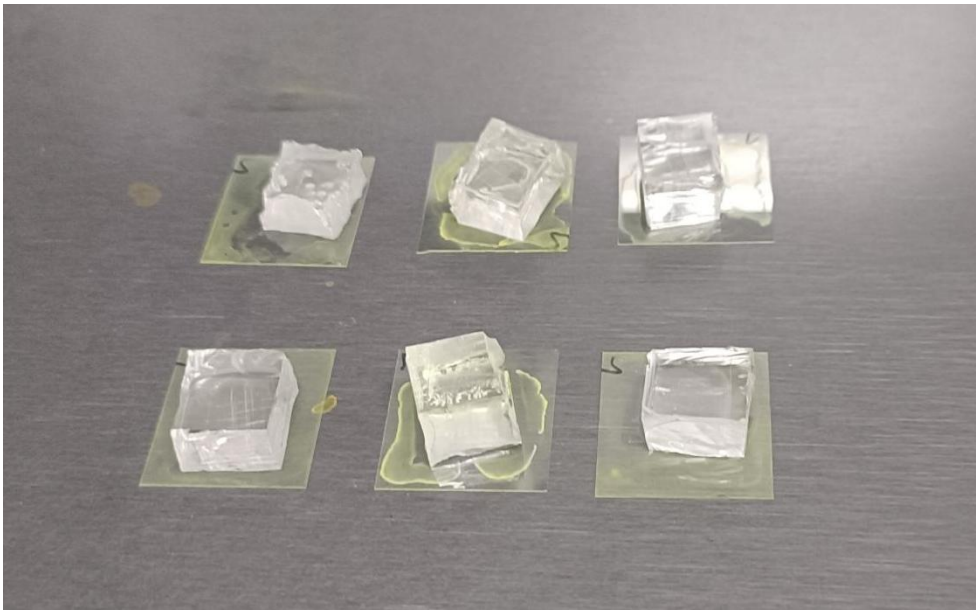

Fig. S12 PDMS-confined solution-growth strategy presentation diagram.

Fig. S13

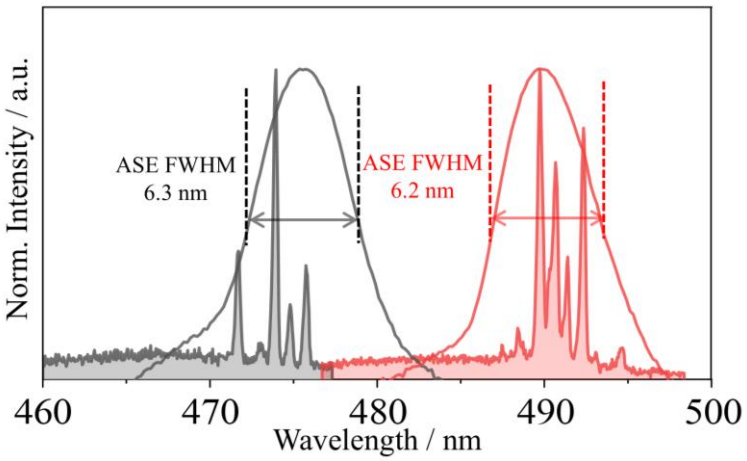

Fig. S13 The spectra of ASE and laser with $Cl_{0.45}Br_{0.55}$ and $Cl_{0.22}Br_{0.78}$.

Fig. S14

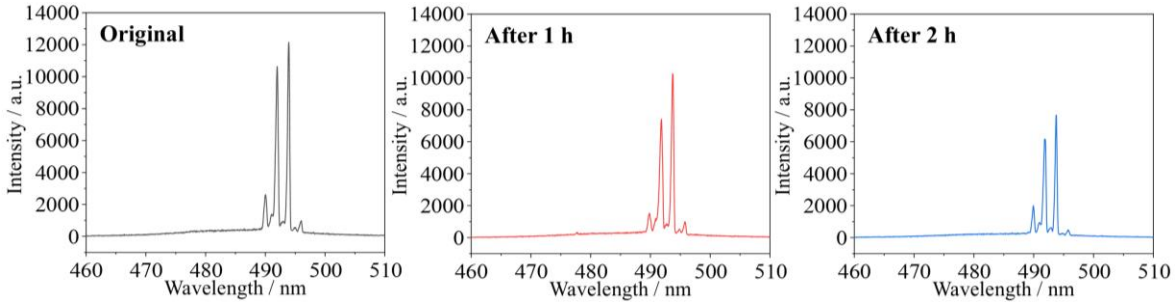

Fig. S14 Spectral stability test by extending the duration of optical pumping from PVP-modified $BA_2Cs_{n-1}Pb_nX_{3n+1}$ micro-ring.

Fig. S15

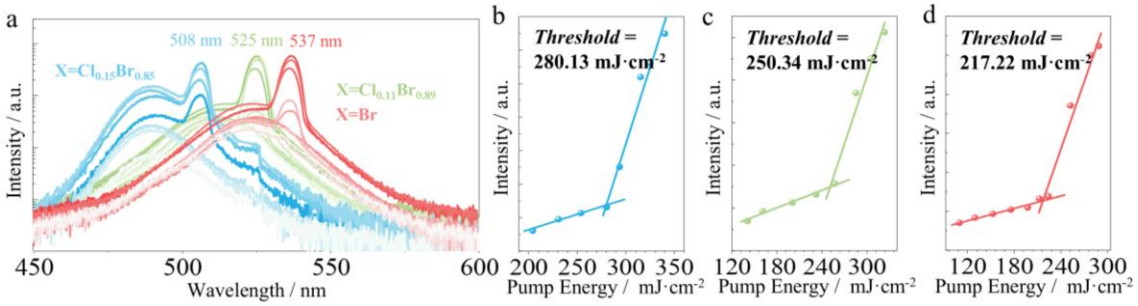

Fig. S15 (a) Nanosecond-pulsed pump-fluence dependent PL intensity of X= $Cl_{0.15}Br_{0.85}$, $Cl_{0.11}Br_{0.89}$ and pure Br films at 355 nm excitation. (b-d) The plot of integrated PL intensities versus pump density of X= $Cl_{0.15}Br_{0.85}$, $Cl_{0.11}Br_{0.89}$ and pure Br films.

Fig. S16

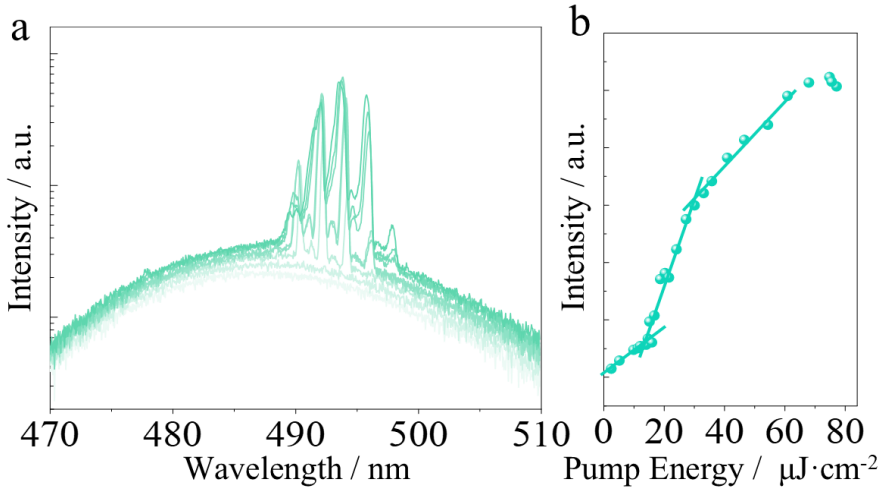

Fig. S16 (a) Pump-fluence-dependent PL intensity from $Cl_{0.22}Br_{0.78}$ micro-rings. (b) The plot of integrated PL intensities versus pump density.

Table S1. The fitting parameters for the decay kinetics of GSB features with different *n*-values in PVP-modified quasi-2D perovskite $BA_2Cs_{n-1}Pb_nX_{3n+1}$.

	GSB$_{n=2}$	**GSB$_{n=4}$**	**GSB$_{n\sim\infty}$ (decay)**	**GSB$_{n\sim\infty}$ (generate)**
Peak/nm	420	475	485	485
τ_1/ps	0.11	0.35	92.37	0.51
τ_1%	59.41%	25.67%	9.28%	100%
τ_2/ps	1.74	6.07	1660.36	-
τ_2%	40.59%	74.33%	90.72%	-
τ_{ave}/ps	0.77	4.60	1514.86	0.51

Table S2. The summary of different blue-green lasers.

Spectral region	Material	Pump source	λ /nm	Threshold /μJ cm^{-2}	Reference
<450nm	$BA_2Cs_{n-1}Pb_nCl_{3n+1}$	340 nm, 250 fs, 1 kHz	425	~25	2021[1]
450-500nm	$CsPb(Cl/Br)_3$	400 nm, 100 fs, 1 kHz	~475	~50	2015[2]
	$CsPbX_3$	400 nm, 100 fs, 1 kHz	~480	~9	2015[3]
	$CsPbCl_{1.6}Br_{1.4}$	400 nm, 100 fs, 1 kHz	470	35.6	2020[4]
	$CsPbBr_{2.25}Cl_{0.75}$	355 nm, 70 fs, 15 Hz	498	45	2021[5]
	$DPEA_2Cs_{n-1}Pb_n(Cl/Br)_{3n+1}$	355 nm, 80 fs, 1 kHz	480	6.5	2022[6]
	$OA_2(Rb/Cs)_{n-1}Pb_nBr_{3n+1}$	400 nm, 200 fs, 1 kHz	484	13.5	2024[7]
	$BA_2Cs_{n-1}Pb_nX_{3n+1}$	**400 nm, 180 fs, 6 kHz**	**477**	**38.39**	**This work**
	$BA_2Cs_{n-1}Pb_nX_{3n+1}$	**400 nm, 180 fs, 6 kHz**	**489**	**23.57**	**This work**
	$BA_2Cs_{n-1}Pb_nX_{3n+1}$	**400 nm, 180 fs, 6 kHz**	**496**	**16.74**	**This work**

Spectral region	Material	Pump source	λ /nm	Threshold /μJ cm^{-2}	Reference
500-550nm	$BA_2Cs_{n-1}Pb_nCl_{3n+1}$	340 nm, 250 fs, 1 kHz	~520	/	2021[1]
	$DPEA_2Cs_{n-1}Pb_n(Cl/Br)_{3n+1}$	355 nm, 80 fs, 1 kHz	~513	/	2022[6]
	$OA_2(Rb/Cs)_{n-1}Pb_nBr_{3n+1}$	400 nm, 200 fs, 1 kHz	~510	/	2024[7]
	$NMA_2FA_{n-1}Pb_nX_{3n+1}$	400 nm, 150 fs, 1 kHz	530	8.5	2018[8]
	$BA_2MA_{n-1}Pb_nBr_{3n+1}$	400 nm, 150 fs, 1 kHz	~542	13.6	2018[9]
	$OA_2MA_{n-1}Pb_nBr_{3n+1}$	400 nm, 100 fs, 1 kHz	548	17.8	2018[10]
	$PEA_2FA_{n-1}Pb_nBr_{3n+1}$	400 nm, 150 fs, 1 kHz	542	4	2020[11]
	$BA_2Cs_{n-1}Pb_nBr_{3n+1}$	340 nm, 250 fs, 1 kHz	~535	7.2	2021[1]
	$BA_2Cs_{n-1}Pb_nX_{3n+1}$	**400 nm, 180 fs, 6 kHz**	**505**	**16.82**	**This work**
	$BA_2Cs_{n-1}Pb_nX_{3n+1}$	**400 nm, 180 fs, 6 kHz**	**510**	**16.89**	**This work**
	$BA_2Cs_{n-1}Pb_nX_{3n+1}$	**400 nm, 180 fs, 6 kHz**	**530**	**12.21**	**This work**

Table S3. Summary of the ASE thresholds of the quasi-2D perovskite $BA_2Cs_{n-1}Pb_nX_{3n+1}$ thin films.

$Cl_{0.45}Br_{0.55}$	**Threshold /μJ·cm^{-2}**	**$Cl_{0.30}Br_{0.70}$**	**Threshold /μJ·cm^{-2}**	**$Cl_{0.22}Br_{0.78}$**	**Threshold /μJ·cm^{-2}**
1	37.06	**1**	23.18	**1**	17.14
2	38.92	**2**	24.68	**2**	17.27
3	37.55	**3**	23.97	**3**	18.22
4	38.68	**4**	22.89	**4**	16.47
5	39.12	**5**	23.9	**5**	16.97
6	38.39	**6**	23.57	**6**	16.74
Average	38.28666667	**Average**	23.69833333	**Average**	17.11833333
SD	0.813428956	**SD**	0.63508792	**SD**	0.607783673
$Cl_{0.45}Br_{0.55}$	**Threshold /μJ·cm^{-2}**	**$Cl_{0.11}Br_{0.89}$**	**Threshold /μJ·cm^{-2}**	**Br**	**Threshold /μJ·cm^{-2}**
1	17.26	**1**	15.86	**1**	11.92
2	17.55	**2**	17.17	**2**	12.96
3	16.14	**3**	17.05	**3**	12.9
4	17.08	**4**	17.25	**4**	12.44
5	17.95	**5**	16.14	**5**	11.85
6	16.82	**6**	16.89	**6**	12.21
Average	17.13333333	**Average**	16.72666667	**Average**	12.38
SD	0.623591747	**SD**	0.582569023	**SD**	0.475773055

Supplemental references

1. J. M. Pina, D. H. Parmar, G. Bappi, C. Zhou, H. Choubisa, M. Vafaie, A. M. Najarian, K. Bertens, L. K. Sagar, Y. Dong, Y. Gao, S. Hoogland, M. I. Saidaminov and E. H. Sargent, *Adv. Mater.*, 2021, **33**, 2006697.
2. Y. Wang, X. Li, J. Song, L. Xiao, H. Zeng and H. Sun, *Adv. Mater.*, 2015, **27**, 7101.
3. S. Yakunin, L. Protesescu, F. Krieg, M. I. Bodnarchuk, G. Nedelcu, M. Humer, G. De Luca, M. Fiebig, W. Heiss and M. V. Kovalenko, *Nat. Commun.*, 2015, **6**, 8056.
4. H. Zhang, J. Yao and H. Fu, *Chem. Mater.*, 2020, **32**, 9602.
5. S. M. H. Qaid, H. M. Ghaithan, B. A. Al-Asbahi and A. S. Aldwayyan, *J. Phys. Chem. C*, 2021, **125**, 9441.
6. C. Wang, G. Dai, J. Wang, M. Cui, Y. Yang, S. Yang, C. Qin, S. Chang, K. Wu, Y. Liu and H. Zhong, *Nano Lett.*, 2022, **22**, 1338.
7. G. Lu, X. Wang, X. Jiang, J. Li, M. Zhu, Z. Ma, D. Zhang, Y. Gao, J. Pan, X. Dai, Z. Ye and H. He, *ACS Nano*, 2024, **18**, 23457.
8. M. Li, Q. Gao, P. Liu, Q. Liao, H. Zhang, J. Yao, W. Hu, Y. Wu and H. Fu, *Adv. Funct. Mater.*, 2018, **28**, 1707006.
9. H. Zhang, Q. Liao, Y. Wu, Z. Zhang, Q. Gao, P. Liu, M. Li, J. Yao and H. Fu, *Adv. Mater.*, 2018, **30**, 1706186.
10. R. Wang, Y. Tong, A. Manzi, K. Wang, Z. Fu, E. Kentzinger, J. Feldmann, A. S. Urban, P. Müller-Buschbaum and H. Frielinghaus, *Adv. Opt. Mater.*, 2018, **6**, 1701311.
11. L. Lei, D. Seyitliyev, S. Stuard, J. Mendes, Q. Dong, X. Fu, Y.-A. Chen, S. He, X. Yi, L. Zhu, C.-H. Chang, H. Ade, K. Gundogdu and F. So, *Adv. Mater.*, 2020, **32**, 1906571.